A Comprehensive Framework for the Modelling of Cartesian Force Output in Human Limbs

Marek Sierotowicz[1,2], Nicola Lotti[3], Rüdiger Rupp[4], Lorenzo Masia[3] and Claudio Castellini[1,2]

***Abstract*— Neuromuscular functional electrical stimulation represents a valid technique for functional rehabilitation or, in the form of a neuroprosthesis, for the assistance of neurological patients. However, the selected stimulation of single muscles through surface electrodes remains challenging particularly for the upper extremity. In this paper, we present the MyoCeption, a comprehensive setup, which enables intuitive modeling of the user's musculoskeletal system, as well as proportional stimulation of the muscles with 16-bit resolution through up to 10 channels. The system can be used to provide open-loop force control, which, if coupled with an adequate body tracking system, can be used to implement an impedance control where the control loop is closed around the body posture. The system is completely self-contained and can be used in a wide array of scenarios, from rehabilitation to VR to teleoperation. Here, the MyoCeption's control environment has been experimentally validated through comparison with a third-party simulation suite. The results indicate that the musculoskeletal model used for the MyoCeption provides muscle geometries that are qualitatively similar to those computed in the baseline model.**

I. INTRODUCTION

Functional electrical stimulation (FES) for artificial generation and support of movements through application of electrical currents represents an integral part in the rehabilitation of neurological patients. In the early phase of rehabilitation, FES is an effective tool in a task-specific, restorative therapy program to foster neurological recovery [1]. In the chronic phase after a neurological disease or trauma, FES may be used as a neuroprosthesis for compensation of completely lost or very weak motor functions. Particularly in individuals with cervical spinal cord injury (SCI) and the associated impairments of the reaching and grasping function, FES has been successfully employed for assistance in activities of daily living (ADL), both using trans-cutaneous [2] and intramuscular electrodes [3].

Non-invasive ES applied through surface electrodes is also used in applications outside the medical field, for example VR and AR [4] [5].

The context of rehabilitation can offer some advantages, as the repetitive, task-specific nature of the movements typically performed during a therapy session allows to implement iterative learning, which allows, among other things, to calibrate inertial parameters and to differentiate the user's own volitional efforts from electrical stimulation [6] [7]. However, many of this sort of setup rely heavily on the assumption of repeated movements, and are ill-fitted to aid movements that do not fulfill this assumption. Furthermore, currently available FES systems, both in the medical field and beyond, use static stimulation schemes, which are open-loop in terms of force, in order to generate predefined multi-joint movements. While most setups available can successfully induce specific movements requiring the stimulation of muscle groups directly associated to them in a bijective fashion (see for example [8]), a general-purpose framework able to associate arbitrary movements or force outputs to more than a few stimulated muscle groups, in particular without relying on the assumption of repeated actions, seems to be still missing.

In this paper, we present a musculoskeletal model which enables to intuitively simulate most kinds of muscle groups, and a prototype designed to use this model in order to provide proportional force control through FES on the upper limb of a user on up to 10 channels with a resolution of 16 bits.

A core principle and fundamental goal in the design philosophy of this system is the adaptability to different users. In order to achieve this, the musculoskeletal model should be easily modifiable to better fit each individual, ideally without the need for much anatomical expertise, and if possible even automatically. In this paper, we describe the entirety of the MyoCeption system, with a particular emphasis on the musculoskeletal model which lies at the basis of its control architecture. This model is experimentally validated by comparing it to a third-party OpenSim model of the right upper limb.

II. SYSTEM DESCRIPTION

The MyoCeption's main purpose is to compute the stimulation currents to be injected through each electrode pair so as to induce a generalized force defined in Cartesian terms at a point which is considered to be the user's end-effector. The hardware, as shown in Fig. 1, consists of a wearable stimulation device and compressive jacket, which presses the surface electrodes onto the user's skin. The stimulation currents (pulse width 200 µs, frequency settable from 0.5 Hz to 100 Hz, maximum amplitude up to 70 mA) are generated by three FES devices (2 *TNS SM2 AKS* and 1 *TNS SM 2MF*, Pierenkemper GmbH, Am Geiersberg 6, 35630 Ehringshausen, Germany). An intermediate wirelessly controlled block (the wireless bluetooth module is an *ESP32*

*This work was not supported by any organization

[1]Marek Sierotowicz and Claudio Castellini are with the Institute of Medical Robotics, Friedrich-Alexander Universität Erlangen-Nürnberg, 91052 Erlangen, Germany marek.sierotowicz@fau.de

[2]Marek Sierotowicz and Claudio Castellini are also with the Institute of Robotics and Mechatronics, German Aerospace Center, 82234 Wessling, Germany

[3]Nicola Lotti and Lorenzo Masia are with the Institute for Technical Informatics (ZITI), Heidelberg University, 69120 Heidelberg, Germany.

[4]Rüdiger Rupp is with the Spinal Cord Injury Center, Heidelberg University Hospital, 69118 Heidelberg, Germany

 DOI: 10.1109/ICORR55369.2022.9896547

Wroom 32, Espressif systems) modulates the generated currents in amplitude from 0 A to the maximum amplitude set on the FES device. The levels of stimulation for each channel are calculated by a remote host computer running an interface software and the MyoCeption Control Environment (MCE). Additionally, the BodyRig [9], a wireless IMU-based body tracking system, is employed. The BodyRig allows to track the body pose with high precision, aligning the musculoskeletal model to the user's posture. Thus, the MCE is provided with the approximated geometry of the user's muscle groups.

Within the MCE, each stimulated muscle group is represented by a line of action going through 4 points ($\vec{p}_1$ to $\vec{p}_4$) plus the origin ($\vec{p}_0$), as shown in Fig. 2.

It is important to notice that, as FES applied through adhesive electrodes typically can not selectively target single muscle groups, there is no bijective mapping from a given line of action in the MCE to a muscle group in the anatomical sense. Rather, each line of action in the MCE is supposed to represent the combined action of all muscle groups stimulated by an electrode pair, and can therefore be seen as a weighted average of the lines of action of the anatomical stimulated muscle groups. The main aim of the analysis presented here, besides comparing different routing methods for the lines of action around different joints, is to confirm this claim. This simplification makes the muscle geometry less computationally expensive, and should ideally make the model easier to fit to an individual user. To this end, future work will focus on perfecting a calibration procedure which should adjust the routing points of each line of action based on recorded twitch movements or torques originating from stimulation of each individual muscle group.

The cumulative moment arm $\vec{r}$ over the entire line of action about the joint $\vec{j}$ is computed according to the following relation

$$\vec{r} = \frac{1}{4}\sum_{i=1}^{4}(\vec{p}_i - \vec{j}) \times \left(\frac{\vec{p}_i - \vec{p}_{i-1}}{||\vec{p}_i - \vec{p}_{i-1}||}\right). \quad (1)$$

This model works under the assumption that the pulling force of the muscle f_m is homogeneous along the whole line of action, which is the case in static conditions. Under this assumption, the force can be considered a scalar, and the torque generated by the muscle is simply the moment arm vector as defined in equation 1 multiplied by f_m. Therefore, overall magnitude of the torque $\vec{\tau}_m$ generated at the joint level by the muscle group m itself can be computed as a function of the moment arm length and of the magnitude of the force f_m pulling along the line of action according to

$$||\vec{\tau}_m|| = ||\vec{r} f_m|| = ||\vec{r}||f_m, \quad (2)$$

where $\vec{r}$ indicates the moment arm vector of a muscle group acting on the joint j as described in equation 1. The moment arm is therefore of high importance for the smooth control of the force output at the user's end-effector over different postures.

The muscle geometry is used to calculate the muscle force needed in order to output an arbitrary generalized force in

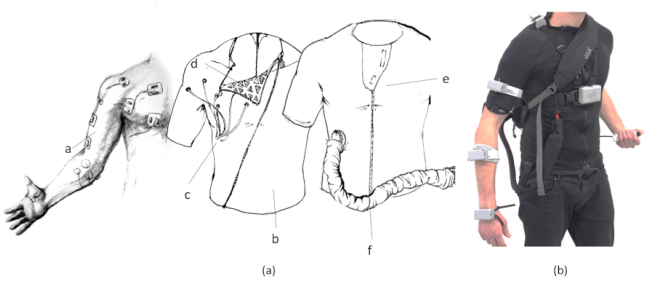

Fig. 1. **a:** MyoCeption system elements. In the picture, from left to right, one can see the surface electrodes applied to the user's skin, which are fitted with Velcro hooks on the outside (a). The inner compression jacket (b) features holes (c) to run the electrode cables through, and is fitted with Velcro loops on the inside, so as to ease electrode application (d). The outer jacket (e) groups the cables in a single umbilical (f) connected to the control electronics, and provides further compression. **b:** Picture of the full setup as worn by a user.

Cartesian terms. In particular, from a desired wrench at the end-effector $\vec{w}_{ee}$, the system calculates the corresponding torques at each joint $\vec{\tau}_j$ through the arm's Jacobian to that joint J^j_{arm} according to the following equation

$$\vec{\tau}_j = J^{jT}_{arm}\vec{w}_{ee}. \quad (3)$$

The single stimulation currents are then computed in order to generate the linear combination of muscular joint outputs $\vec{\tau}_m$ acting on the joint j that best approximates the desired joint torque $\vec{\tau}_j$. The kind of linear combination depends on the selected muscle recruitment strategy. For instance, in the case of a nearest neighbour recruitment strategy, only the muscle group with the torque output $\vec{\tau}_m$ closest in direction to the desired joint torque $\vec{\tau}_j$ is stimulated. Other strategies could employ a suitable pseudo-inverse of the muscular Jacobian, or its transpose in the case of an admittance controller. The intensity of the stimulation also depends on the expected effect of the stimulation current on the muscular force f_m.

Different routings of the lines of action are possible. In particular, here we examine a simple line-of-sight routing, a routing similar to the one presented in [10], and a third one. From this point on, these routings will be referred to as *line of sight*, *sphere projection* and *shifted sphere projection*, respectively.

The line of sight routing, shown in Fig. 2 left, simply connects the origin point $\vec{p}_0$ (the most proximal point of the line of action) to the insertion point $\vec{p}_4$ (the most distal point of the line of action) with a straight line. The line of action of many muscle groups can be well approximated through such a routing, and because of its simplicity, it is used within the MCE any time a line of sight exists between the origin and the insertion point. However, this routing can not accurately model any line of action going around a joint, as is the case, e.g., for the triceps in most postures.

The sphere projection routing, shown at the center in Fig. 2, routes the line of action through via points co-planar to the joint and the line of action's origin and insertion (shown in the figure as $\vec{p_1}$ and $\vec{p_3}$). The routing connects the two

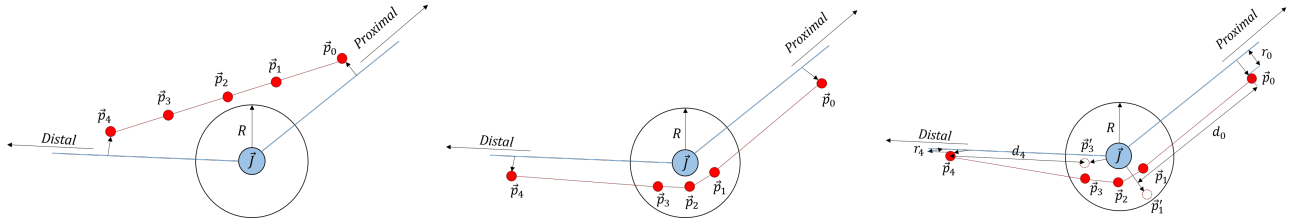

Fig. 2. Illustration of the line of sight routing (left), the sphere projection routing (center), and the shifted sphere projection routing (right).

via points closest to the joint with a straight line if said line does not enter a sphere of radius R with the joint lying at its center. If, on the other hand, the line of sight does intersect the sphere, then the line of action is routed through a point $\vec{p}_2$, which is the point on the line of sight that is closest to the joint projected onto the sphere in the radial direction.

In the MCE, this method can lead to problems if the $\vec{p}_0$ and $\vec{p}_4$ points lie far away from the joint relative to the sphere's radius R. An example of this problem is shown in Fig. 3. The figure shows the difference in orientation of the expected torque output from the line of action corresponding to the elbow extenders when the line is routed through the shifted sphere projection and when it is routed through sphere projection. Ideally, the torque output should be aligned with the elbow axis $\vec{e}$, but as shown in the figure, this can sometimes not be the case when using sphere projection routing. In [10], this problem presumably doesn't present itself because the via points are based on MRI imaging, and can therefore be precisely placed with high spatial accuracy even in close proximity of the joint. In [11], where a routing similar to sphere projection is used to predict the kinematics of a tendon-actuated tremor-suppressing glove, this is not an issue, as the tendons pass through guides which are very close to the user's joints. If the joint is modeled as having a single rotational degree of freedom, a possible solution would be to then project the torque onto the joint's axis, or even use a cylinder of radius R with its axis aligned with that of the joint instead of a sphere. However, if the direction of the axis is itself not known with certainty, this solution is not viable.

The shifted sphere projection routing, shown in Fig. 2 on the right, consists of the following steps.

- Compute the points $\vec{p}_1'$ and $\vec{p}_3'$. These are points obtained by shifting $\vec{p}_0$ and $\vec{p}_4$ along the respective link towards the joint $\vec{j}$ until they are closest to it, and by then projecting them in the radial direction onto the sphere of radius R with the joint lying at its center.
- The point $\vec{p}_2$ is the closest point on the sphere from $\vec{p}' = \frac{(\vec{p}_1' + \vec{p}_3')}{2}$.
- Finally, the points $\vec{p}_1$ and $\vec{p}_3$ are the point on the sphere closest to the projections of $\vec{p}_1'$ and $\vec{p}_2'$ on the planes defined by $\left\langle \vec{p}_0, \vec{j}, \vec{p}_2 \right\rangle$ and $\left\langle \vec{p}_4, \vec{j}, \vec{p}_2 \right\rangle$, respectively.

As shown in Fig. 3, shifted sphere projection can give a more consistent torque direction than the sphere projection routing for lines of action whose origin and insertion points lie far from the joint relative to the sphere's radius R. However, shifted sphere projection cannot transition to line of sight without discontinuities, which is possible using the sphere projection routing. Such discontinuities are shown in Fig. 5.

III. EXPERIMENTAL PROTOCOL

In order to validate the MCE, a comparison was drawn between the MyoCeption's musculoskeletal model and an OpenSim Dynamic Arm Simulator model (DAS) [12] shown on the right in Fig. 4, which simulates the musculature responsible for the movements of the right upper limb in detail. OpenSim is widely used as a modelling tool in bio-mechanics, and can boast a vast community creating simulations and models for a diverse range of applications.

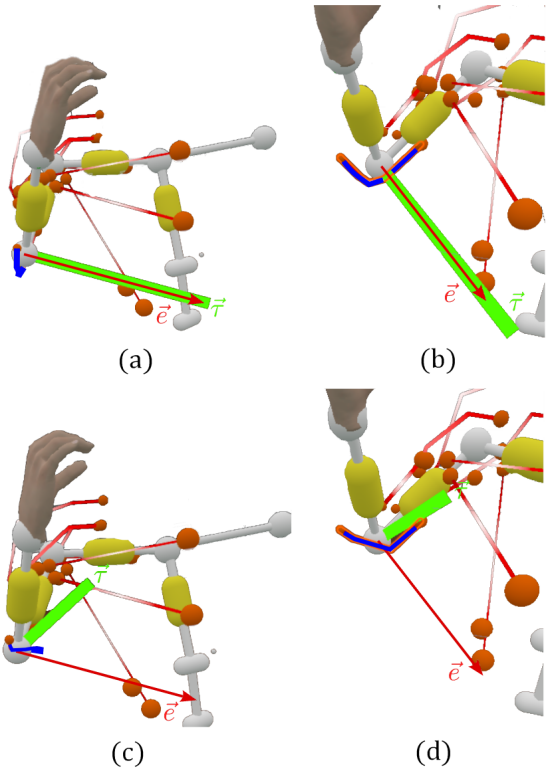

Fig. 3. Issue with the sphere projection routing. In this example, a line of action within the MCE close in position to the *triceps brachii*, highlighted in blue, is shown with the direction of the torque it can exert on the elbow joint (shown as a green line and labeled as $\vec{\tau}$). **a** and **b:** the action line is routed using shifted sphere projection. The expected torque is aligned with the elbow's axis (red arrow marked $\vec{e}$). **c** and **d:** the sphere projection routing is used instead. Notice how the action line passes on the side, and this causes the expected torque direction $\vec{\tau}$ to deviate from the elbow's axis $\vec{e}$.

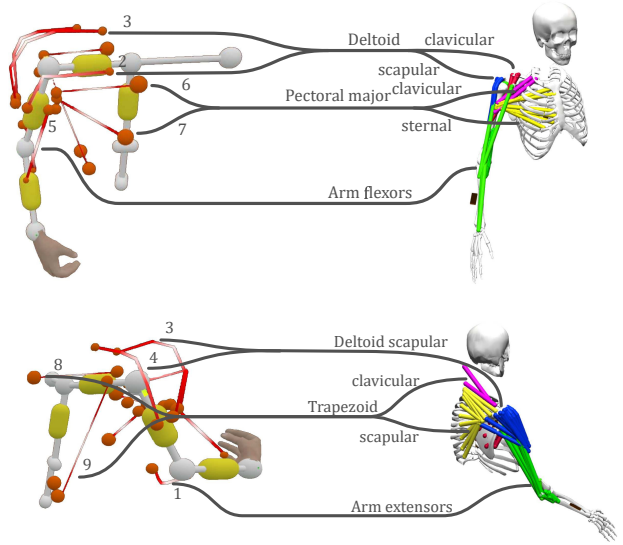

Fig. 4. The two musculoskeletal models to be compared. On the left is the MyoCeption Control Environment, on the right the Dynamic Arm Simulator implemented in OpenSim. The action lines of the MCE are designated by channel number, while the DAS muscle groups are designated by name and differentiated by color. The grey lines represent the assumed correspondences between the DAS muscle groups and the MCE stimulation channels based on positional proximity and on the joint about which each line of action operates.

The data set for the comparison was recorded with the body tracking system from [9]. One able-bodied user (age 27, 1.87m, 85kg) performed elbow flexion/extension, shoulder flexion/extension, and shoulder adduction/abduction over 4 repetitions in real time. The postures during these movements were used to align both the MCE and the DAS kinematics. The moment arm of the involved muscle groups were compared across the recorded movements between the two. The moment arm length $||\vec{r}||$ of the lines of action is the effective moment arm of the muscle group.

In order to test the claim that each line of action in the MCE could be seen as a weighed average of all muscle groups stimulated by an electrode pair, here we executed a multivariate regression from the moment arms in the DAS to the moment arms of the MCE assumed to correspond to them. Here we focus on demonstrating a qualitative similarity between the two models. Therefore, we would expect high correlation between the moment arm length corresponding to the lines of action in the MCE and the muscle groups that are closest in position in the DAS. The assumed correspondences between the DAS muscle groups and the MCE lines of action are shown in Fig. 4. This analysis is also used to evaluate which routing method would provide the better qualitative correlation of the muscle's lever arm between the MCE and the OpenSim DAS model.

IV. RESULTS

The evaluated metrics from the multivariate regression performed from the moment arm lengths of the DAS muscle groups onto the moment arm lengths of the MCE lines of action are the squared Pearson's correlation coefficient R^2 and the root mean square error (RMS) normalized by the maximum difference of the moment arm from its mean. This normalization has the purpose of representing the RMS as a fraction of the maximum range of the regression target. Table I gathers the result of the multivariate regression analysis from each DAS muscle group involved in the movements performed during the experiment to the MCE stimulation channels assumed to correspond to them, according to Fig. 4. The results are sorted by the movements performed during the experiment. In Fig. 5, the moment arm on the MCE stimulation channel 2, routed using shifted sphere projection, is shown and compared to the moment arm of the DAS deltoid clavicular. Fig. 6 shows the moment arm length of the MCE line of action closest to the biceps brachii in the DAS over the elbow flexion angle, as well as the moment arm length of the DAS biceps brachii itself. For ease of comparison, the curve shown in Fig. 6 is not obtained aligning the DAS to the IMU data, but rather shows a sweep of the moment arm length over the full range of the elbow flexion angle, which in the OpenSim model can be freely set.

TABLE I

MULTIVARIATE REGRESSION RESULTS.

MCE	DAS	Movement	R^2	RMS
5	Elbow flexors	Elbow flex/ext	0.917	0.152
1	Elbow extenders	Elbow flex/ext	0.96	0.100
2	delt clav	Sh. add/abd	0.940	0.152
2	delt scap	Sh. add/abd	0.960	0.124
3	delt clav	Sh. add/abd	0.879	0.190
3	delt scap	Sh. add/abd	0.910	0.164
4	delt scap	Sh. add/abd	0.917	0.103
2	delt clav	Sh. flex/ext	0.904	0.140
3	delt clav	Sh. flex/ext	0.906	0.140
4	delt clav	Sh. flex/ext	0.967	0.100
2	delt scap	Sh. flex/ext	0.906	0.139
3	delt scap	Sh. flex/ext	0.969	0.081
4	delt scap	Sh. flex/ext	0.971	0.094
6	pect maj c	Sh. flex/ext	0.736	0.147
7	pect maj c	Sh. flex/ext	0.783	0.219
6	pect maj t	Sh. flex/ext	0.886	0.097
7	pect maj t	Sh. flex/ext	0.836	0.190
8	trap clav	Sh. flex/ext	0.879	0.131
9	trap clav	Sh. flex/ext	0.534	0.228
8	trap scap	Sh. flex/ext	0.868	0.077
9	trap scap	Sh. flex/ext	0.971	0.121

V. DISCUSSION

While the shifted sphere projection routing seems to more robustly model line of action torque output where the origin and the insertion points are far away from the joint relative to the joint's sphere diameter R, it is unable to transition to a line-of-sight routing without discontinuities when the line of action does not go around a joint. This effect is shown in Fig. 5. The discontinuities in the moment arm length from the MCE are clearly visible. These happen due to the transition of the routing from shifted sphere to line of sight. This leads to generally poor correlations between the two

models for all muscle groups where such a transition occurs during movement. This, in particular, is the case for the lines of action corresponding to the deltoids, for which it happens that the line of sight from the origin and the insertion point can run outside of the joint sphere during shoulder abduction or shoulder flexion.

Using the sphere projection routing on the lines of action corresponding to the deltoids in the MCE leads to high correlation coefficients on the moment arm lengths both during shoulder adduction/abduction and shoulder flexion/extension, as shown in Table I.

Finally, Fig. 6 shows the moment arm length of the biceps brachii of the DAS, as well as the moment arm length of the closest action line in the MCE, which is routed using line-of-sight. The moment arm length of the two muscle groups are normalized by the respective maximum to ease the comparison. As shown in Table I, the moment arm of the MCE lines of action going over the elbow joint are well represented by a weighed sum of the moment arms of the DAS elbow flexors and extensors. Looking at this comparison between two specific lines of action, it seems that the curves look qualitatively very similar, showing only a discrepancy in the angle for which the curve's maximum occurs. By adjusting only a few parameters through a suitable calibration procedure, the similarity could be improved. In general, the multivariate regression shows a good fit of the moment arms as computed by the MCE with the regression model based on the DAS muscle groups, with the main exception of action line 9, which shows a poor fit with the linear model with the trapezoid clavicular group from the DAS. This could perhaps be explained by the relative distance in position between the two muscle groups in the models, as shown in Fig. 4.

The good fit of the multivariate regression indicates that the moment arm length of the lines of action in the MCE can be well explained by the moment arm lengths in the DAS. This confirms that the MCE is able to compute qualitatively similar moment arms over the motions examined in this experiment as those computed in the DAS. As the moment arms are fundamental in the estimation of the torque output associated to each line of action, this is a indispensable validation for the MCE. Furthermore, the results shown here suggest that shifting the origin and insertion points of the lines of action in the MCE could account for stimulation

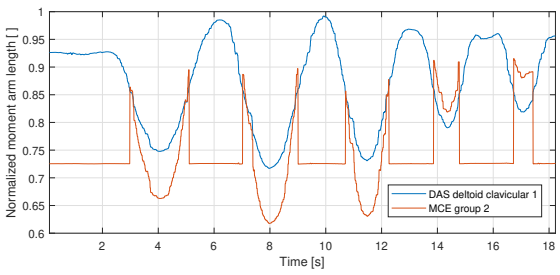

Fig. 5. Moment arm length of the MCE muscle group 2 and the deltoid clavicular group 1 from the DAS using the shifted sphere projection routing.

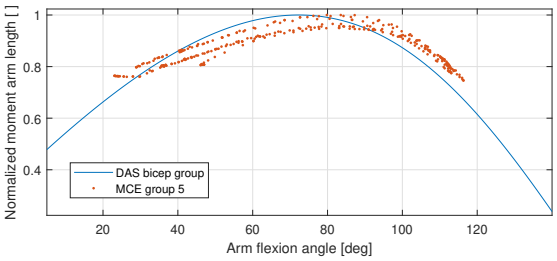

Fig. 6. Comparison of the moment arm of the bicep group 1 from the DAS and the MCE line of action 5, which is modeled using line of sight routing, over the elbow flexion angle.

currents hitting different muscle groups than the anticipated ones. This can be inferred by looking, e.g., to the better fit between the trapezoid clavicular group from the DAS and the MCE line of action 8, as opposed to the MCE line of action 9, as shown in Table I. In a hypothetical scenario where the stimulation current associated with the MCE line of action 9 exclusively hits the trapezoid clavicular, shifting the line of action 9 to be closer to the line of action 8 would ensure a more accurate calculation of the torque output deriving from this stimulation. Future work will focus on calibration procedures able to accomplish such an adjustment automatically based on data acquired on human users.

VI. CONCLUSIONS

The present article serves as a presentation of the MyoCeption system, and as a validation of the system's control environment. A comparison with a third-party, detailed model of the human upper limb shows that the musculoskeletal model governing the MyoCeption's control system, while being simpler and not requiring almost any anatomical expertise to be set up, is able to compute the salient characteristics of the muscle geometry to a comparable degree.

Furthermore, the comparison between MCE and DAS allowed to evaluate the advantages and disadvantages of the three proposed line of action routings. In particular, the line-of-sight routing is very simple, and could be easily adjusted to fit the effective moment arm length of an arbitrary user's muscle measured over the range of motion of a given joint. However, the line of action of most muscles can not be approximated as a straight line, especially if the line of action passes around a joint. The sphere projection routing does allow for transition without discontinuities in the moment arm's length between a state where the line of action goes around a joint and a state where a line of sight exists between origin and insertion point. However, the sphere projection routing seems to not be particularly robust to inaccuracies in the placement of the via points $\vec{p}_1$ and $\vec{p}_3$. The shifted sphere projection does not allow for continuous transition to a line of sight state, which leads to discontinuities that could be extremely problematic when this routing is used to compute the amount of stimulation current to be injected into a user. However, this routing seems more robust with respect to the placement of the origin and insertion point of the line of action. It would therefore be advisable to use this routing

for lines of action which are not expected to have a line-of sight between their origin and their insertion, independent of the user's posture.

This test suffers from a few limitations. In particular, here we showed only a qualitative correlation between the moment arm lengths of the two musculoskeletal models. No effort was put into verifying whether the MyoCeption's control environment provides values close in value to those that would be measured in reality for a given user. The results presented by Hainisch et Al. in [10] show that, even when fitting the muscular lines of action to MRI data in an OpenSim model, the torque output computed by the calibrated model can show noticeable discrepancies with data acquired directly on humans over joint movements. Therefore, a model such as the DAS is not necessarily the best possible ground truth, and future work should focus on the comparison of the MCE model with data gathered *in vivo*, and on improving the fitness of the model in a quantitative sense as well. Furthermore, here the MCE has been verified just for single-joint movements and not for movements involving more than one joint. In such cases, the geometry of biarticular muscles in particular could change noticeably, and lead to discrepancies between the ground truth and the MCE model.

Besides the offline comparison of the MCE with other models or data gathered *in vivo*, future work will also focus on closing the real-time control loop in force. In order to do so, a few possibilities exist. In particular, the integration of further sensor modalities in the system, such as force and torque, would allow to monitor the applied forces on each joint during movements, and optimize the model's parameters accordingly. Such measurement modalities could be added to the system by fitting it with a passive or even an active sensor-fitted exoskeleton or exosuit. Therefore, the interaction of the MyoCeption's FES setup and such rehabilitative robotic systems shall be investigated.

In [13], Anaya et al. present many examples of hybrid FES-robotic gait rehabilitation technologies, mostly based on rigid exoskeletons used in conjunction with electrical stimulation. The MCE could be employed in such setups also on upper limbs: the pulling vector estimation could be used to generate force fields in rehabilitation robotics that mimic the effect of a single musculutendon unit or a muscle group [14].

In the context of soft wearable exosuit control, on the other hand, the MCE could be used to extend the so called *Myoprocessor* presented in [15] to multiple degrees of freedom in order to assist both the elbow and the shoulder. In conjunction with FES, an exosuit controlled through the MCE could be more effective in restoring motor function in the presence of chronic neuromuscular diseases. Future steps will test the presented approach in exosuit control both in clinical and industrial settings [16].

Regarding the MCE's use in VR and AR, future studies will involve a bimanual rigid exoskeleton [17] with MyoCeption-driven haptic rendering in order to improve immersiveness of a simulation.

References

[1] N. Kapadia, B. Moineau, and M. R. Popovic, "Functional electrical stimulation therapy for retraining reaching and grasping after spinal cord injury and stroke," *Frontiers in Neuroscience*, p. 718, 2020.

[2] R. Rupp, M. Rohm, M. Schneiders, A. Kreilinger, and G. R. Müller-Putz, "Functional rehabilitation of the paralyzed upper extremity after spinal cord injury by noninvasive hybrid neuroprostheses," *Proceedings of the IEEE*, vol. 103, no. 6, pp. 954–968, 2015.

[3] A. B. Ajiboye, F. R. Willett, D. R. Young, W. D. Memberg, B. A. Murphy, J. P. Miller, B. L. Walter, J. A. Sweet, H. A. Hoyen, M. W. Keith, *et al.*, "Restoration of reaching and grasping in a person with tetraplegia through brain-controlled muscle stimulation: a proof-of-concept demonstration," *Lancet (London, England)*, vol. 389, no. 10081, p. 1821, 2017.

[4] P. Lopes and P. Baudisch, "Interactive systems based on electrical muscle stimulation," *Computer*, vol. 50, no. 10, pp. 28–35, 2017.

[5] P. Lopes, S. You, A. Ion, and P. Baudisch, "Adding force feedback to mixed reality experiences and games using electrical muscle stimulation," in *Proceedings of the 2018 chi conference on human factors in computing systems*, 2018, pp. 1–13.

[6] K. L. Meadmore, A.-M. Hughes, C. T. Freeman, Z. Cai, D. Tong, J. H. Burridge, and E. Rogers, "Functional electrical stimulation mediated by iterative learning control and 3d robotics reduces motor impairment in chronic stroke," *Journal of neuroengineering and rehabilitation*, vol. 9, no. 1, pp. 1–11, 2012.

[7] C. Freeman, T. Exell, K. Meadmore, E. Hallewell, and A.-M. Hughes, "Computational models of upper-limb motion during functional reaching tasks for application in fes-based stroke rehabilitation," *Biomedical Engineering/Biomedizinische Technik*, vol. 60, no. 3, pp. 179–191, 2015.

[8] C. Freeman, A. Hughes, J. Burridge, P. Chappell, P. Lewin, and E. Rogers, "A model of the upper extremity using fes for stroke rehabilitation," *Journal of Biomechanical Engineering*, vol. 131, no. 3, 2009.

[9] M. Sierotowicz, M. Connan, and C. Castellini, "Human-in-the-loop assessment of an ultralight, low-cost body posture tracking device," *Sensors*, vol. 20, no. 3, p. 890, 2020.

[10] R. Hainisch, M. Gfoehler, M. Zubayer-Ul-Karim, and M. G. Pandy, "Method for determining musculotendon parameters in subject-specific musculoskeletal models of children developed from mri data," *Multibody System Dynamics*, vol. 28, no. 1, pp. 143–156, 2012.

[11] P. Daemi, Y. Zhou, K. Inzunza, M. D. Naish, A. D. Price, and A. L. Trejos, "Kinematic modeling and characterization of a wearable tremor suppression device for pathological tremor reduction," in *2020 8th IEEE RAS/EMBS International Conference for Biomedical Robotics and Biomechatronics (BioRob)*. IEEE, 2020, pp. 1236–1241.

[12] E. K. Chadwick, D. Blana, R. F. Kirsch, and A. J. Van Den Bogert, "Real-time simulation of three-dimensional shoulder girdle and arm dynamics," *IEEE Transactions on Biomedical Engineering*, vol. 61, no. 7, pp. 1947–1956, 2014.

[13] F. Anaya, P. Thangavel, and H. Yu, "Hybrid fes–robotic gait rehabilitation technologies: a review on mechanical design, actuation, and control strategies," *International journal of intelligent robotics and applications*, vol. 2, no. 1, pp. 1–28, 2018.

[14] N. Lotti and V. Sanguineti, "Emg-driven force fields: Toward a myoprocessor for virtual biomechanics," in *International Conference on NeuroRehabilitation*. Springer, 2018, pp. 1161–1165.

[15] N. Lotti, M. Xiloyannis, F. Missiroli, C. Bokranz, D. Chiaradia, A. Frisoli, R. Riener, and L. Masia, "Myoelectric or force control? a comparative study on a soft arm exosuit," *IEEE Transactions on Robotics*, 2022.

[16] F. Missiroli, N. Lotti, E. Tricomi, C. Bokranz, R. Alicea, M. Xiloyannis, J. Krzywinski, S. Crea, N. Vitiello, and L. Masia, "Rigid, soft, passive, and active: a hybrid occupational exoskeleton for bimanual multijoint assistance," *IEEE Robotics and Automation Letters*, 2022.

[17] E. D'Antonio, E. Galofaro, F. Patané, M. Casadio, and L. Masia, "A dual arm haptic exoskeleton for dynamical coupled manipulation," in *2021 IEEE/ASME International Conference on Advanced Intelligent Mechatronics (AIM)*. IEEE, 2021, pp. 1237–1242.